RSC Advances

PAPER

View Article Online
View Journal | View Issue

Cite this: *RSC Adv.*, 2023, **13**, 20748

On the mechanism of acceptorless dehydrogenation of N-heterocycles catalyzed by ^{t}BuOK: a computational study†

Lishuang Ma,[a] Wenxu Feng,[a] Shidong Zhao,[a] Chuangye Wang,[a] Yanyan Xi[b] and Xufeng Lin *[ab]

Received 27th June 2023
Accepted 4th July 2023

DOI: 10.1039/d3ra04305c

rsc.li/rsc-advances

The catalytic acceptorless dehydrogenation (ADH) of saturated N-heterocycles has recently gained considerable attention as a promising strategy for hydrogen release from liquid organic hydrogen carriers (LOHCs). Recently, a simple ^{t}BuOK base-promoted ADH of N-heterocycles was developed by Yu *et al.* (*Adv. Synth. Catal.* 2019, **361**, 3958). However, it is still open as to how the ^{t}BuOK plays a catalytic role in the ADH process. Herein, our density functional study reveals that the ^{t}BuOK catalyzes the ADH of 1,2,3,4-tetrahydroquinoline (**THQ**) through a quasi-metal–ligand bifunctional catalytic channel or a base-catalyzed pathway with close energy barriers. The hydride transfer in the first dehydrogenation process is determined to be the rate determining step, and the second dehydrogenation can proceed directly from **34DHQ** regulated by the ^{t}BuOK. In addition, the computational results show that the cooperation of a suitable alkali metal ion with the ^{t}BuO^{-} group is so critical that the ^{t}BuOLi and the isolated ^{t}BuO^{-} are both inferior to ^{t}BuOK as a dehydrogenation catalyst.

1. Introduction

Liquid organic hydrogen carriers (LOHCs) have been recognized as promising hydrogen storage media, due to their high hydrogen capacity (5–7.4 wt%), reversibility, moderate dehydrogenation kinetics, relative safety and compatibility with existing infrastructure for fuels.[1] The utilization of N-containing LOHCs has particularly attracted growing attention in recent years as the introduction of N atoms can benefit the dehydrogenation process, both thermodynamically and kinetically, compared to the carbocycle compounds.[2,3] However, the H_2 release process itself is entropically favoured but thermodynamically uphill.[2] In addition, some key factors such as catalytic activity, selectivity, durability as well as heating demand strongly depend on the performance of catalysts. Thus, there is a highly desire to develop efficient catalysts and catalytic strategies for the N-containing LOHC systems.[3]

The catalytic acceptorless dehydrogenation (ADH) is a cornerstone achievement in organometallic catalysis as reviewed by Milstein,[4] which is not only atom-economical with liberation of H_2 and no waste generation, but also environmentally benign without the need of any stoichiometric oxidants or sacrificial acceptors. Given these advantages, the catalytic ADH has been increasingly applied in the LOHC-based hydrogen storage, and significant efforts have been dedicated to developing diverse homogenous and heterogeneous catalysts for ADH of N-heterocycles.[2c,d,5] To date, a series of transition metal catalysts,[5] including the homogenous ones such as Cp*Ir(III),[6,7] Fe(II)-PNP,[8a] Co(II)-PNP,[8b] CpNi(NHC),[9] Ru(II)-NNC,[10] Ru(II)-CNN(H)[11] and Os(IV or II)[12] metal-complex catalysts, and the heterogeneous ones such as Fe,[13] Co[14] and Mn[15] based single-atom and nanoparticle catalysts, have been developed for ADH reactions of N-heterocycles. With the aim of providing low-cost and environmentally benign protocols, the transition-metal-free catalysts represent appealing alternatives, although such catalysts are less exploited, especially under acceptor-free conditions. The heterogenous metal-free carbocatalysts such as nitrogen-assembly carbons (NCs)[16a] and reduced graphene oxides (rGOs)[16b] were demonstrated efficient with high reusability and stability even under ambient temperature. The homogenous $B(C_6F_5)_3$ catalyst was used by Kanai *et al.* in 2016, to catalyze the ADH of N-heterocycles with high functional group tolerance.[17a] The $B(C_6F_5)_3$ was also applied in the frustrated Lewis pair catalyzed ADH of the N-protected indolines, in which a weak Lewis acid acts as the hydride shuttle.[17b] In 2019, the ADHs of 1,2,3,4-tetrahydroquinoline (**THQ**), indoline and their derivatives promoted by only a simple ^{t}BuOK base were efficiently realized by Yu and co-workers, without using any other catalysts or additives in *o*-xylene at 140 °C (see Scheme 1),[18] which offers a transition-metal-free and operationally simple alternative.

[a]*College of Chemistry and Chemical Engineering, China University of Petroleum (East China), Qingdao 266580, P. R. China. E-mail: hatrick2009@upc.edu.cn*

[b]*State Key Laboratory of Heavy Oil Processing, China University of Petroleum (East China), Qingdao 266580, P. R. China*

† Electronic supplementary information (ESI) available. See DOI: https://doi.org/10.1039/d3ra04305c

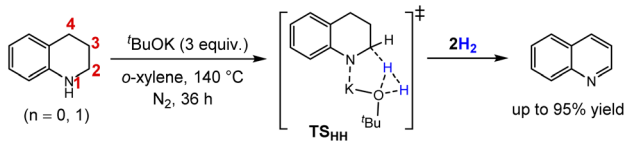

Scheme 1 Acceptorless dehydrogenation of THQ promoted by ^{t}BuOK.[18] Numbering scheme is shown in red for THQ.

Despite the remarkable progress in the experimental investigations on the ADH of N-heterocycles, of equivalent importance is the fundamental understanding to serve for rational catalyst design and optimization.[19,20] Previously, several computational studies demonstrated that the ADH of N-heterocycles catalyzed by Cp*Ir[20a] and Fe-PNP[20b,c] transition metal complexes can operate effectively by the cooperation of metal and ligand, *via* stepwise or concerted proton/hydride transfer pathways. However, the simple ^{t}BuOK catalyzed dehydrogenation additionally complicates the mechanism,[18] since the intrinsic catalytic activities of bases such as ^{t}BuOK were usually neglected in the presence of a transition metal catalyst.[21] In addition, it was previously reported by Berkessel and Muller that the isolated alkali base can catalyze the hydrogenation of ketones, which was proposed to occur *via* a six-membered transition state in which H_2 is activated by bridging ketone and alkoxide (see $\mathbf{TS_{BC}}$ in Scheme 2), based on kinetic studies[22] and inspiration of the metal–ligand bifunctional catalytic mechanism developed by Noyori (see $\mathbf{TS_{MLC}}$ in Scheme 2).[23] This base catalytic mechanism was further revised by Dub *et al.*, who suggested a stepwise pathway in solution where the H–H bond is first activated by ^{t}BuOK to afford a KH intermediate.[24] These raise the questions of how the ^{t}BuOK plays a catalytic role in the dehydrogenation of N-heterocycles, and whether it behaves like a bifunctional transition metal catalyst or that in the base catalyzed hydrogenation reaction.[22–24] Herein, we therefore employed the density functional theory (DFT) method to provide a comprehensive understanding of the ADH pathways of 1,2,3,4-tetrahydroquinoline (**THQ**) catalyzed by a ^{t}BuOK base catalyst.

2. Computational methodology

In the present study, DFT calculations were performed to investigate the ADH mechanism of **THQ** catalyzed by the ^{t}BuOK base catalyst. All minima of the reactants, products as well as intermediates were first obtained by full system optimization, using the B3LYP hybrid density functional[25] including empirical dispersion correction computed with Grimme's D3 formula (B3LYP-D3).[26] The def2-TZVP[27] basis set was applied for all the atoms. The transition states on the energy profiles were obtained by employing the conventional approach of transition state optimization at the same level. Vibrational frequency analysis calculations were also performed for all the optimized structures, to ensure that each stationary point truly represented a local minimum or a saddle point, and to derive the thermochemical corrections for the enthalpies and free energies. To inspect the influence of the calculation level on the relative energies, the energies of some rate-determining intermediates and transition states were refined by single-point energy calculations at the B3LYP-D3/def2-QZVP level of theory. To consider solvent effects, the solvation model based on density (SMD) for *o*-xylene ($\varepsilon = 2.5454$) was employed for all the calculated points at a temperature of 298.15 K. All calculations were carried out by using the Gaussian 09 program package.[28] The non-covalent interaction (NCI) and extended transition state-natural orbitals for chemical valence (ETS-NOCV) analyses were performed by using the Multiwfn programme.[29]

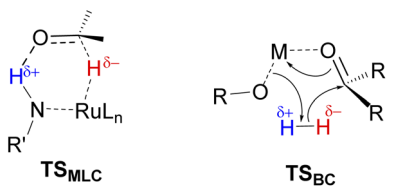

Scheme 2 Key transition states in mechanisms of the metal–ligand bifunctional catalysis ($\mathbf{TS_{MLC}}$) and the base-catalyzed hydrogenation ($\mathbf{TS_{BC}}$).[22,23]

3. Results and discussion

3.1. Dehydrogenation from THQ to DHQ

The tetrameric cubane-type cluster (^{t}BuOK)$_4$ was proposed as the reactive catalytic species in several reports,[30] however, the cubic cluster can dissolve into different small aggregates in protic *tert*-butanol according to the AIMD simulations reported by Dub *et al.*,[24a] and it can be speculated that the result would turn out to be very complicated under high temperature up to 140 °C experimentally.[18] Indeed, it has proven to be practical to study the base catalytic mechanism using a single ^{t}BuOK as the model catalyst.[31] Thus, we commenced this work with an isolated ^{t}BuOK as the catalyst to understand the base catalyzed ADH process of **THQ**. As shown in Fig. 1a, an encounter complex **M1** can be initially formed *via* an N–H···O hydrogen bond with a stabilization energy of 4.1 kcal mol^{-1}. Subsequently, proton migration from N1 to the oxygen atom of ^{t}BuOK occurs by overcoming a tiny free energy barrier (1.8 kcal mol^{-1}) *via* **TS1**. An ion-pair complex **M2** is thus generated after proton transfer, and is 7.6 kcal mol^{-1} in free energy more stable than the separated species. Note that the optimized **M2** is more stable than **TS1** in terms of electronic energy, but higher after thermal corrections. As a result, this process leads to the shortened distance between K$^+$ and H2a (**M1:** 3.82 Å → **M2:** 3.60 Å) as well as the concomitant slightly elongation of C2–H2a bond (1.11 Å in **M1** *versus* 1.09 Å in **THQ**), which is helpful in preparing for the subsequent hydride transfer.

Starting from **M2**, hydride transfer occurs from C2(sp^3)–H2a to K$^+$, *via* the six-membered transition state **TS2** with a sizeable energetic barrier of 34.2–34.5 kcal mol^{-1} (obtained by using B3LYP-D3 functional with def2-TZVP and def2-QZVP basis sets), relative to **M1** according to the energetic span model.[32] In contrast, hydride transfer pathway from the equatorial C2(sp^3)–H2e bond to K$^+$ was calculated to afford an energy barrier 2.9 kcal mol^{-1} higher than the former one (see Fig. S1†),

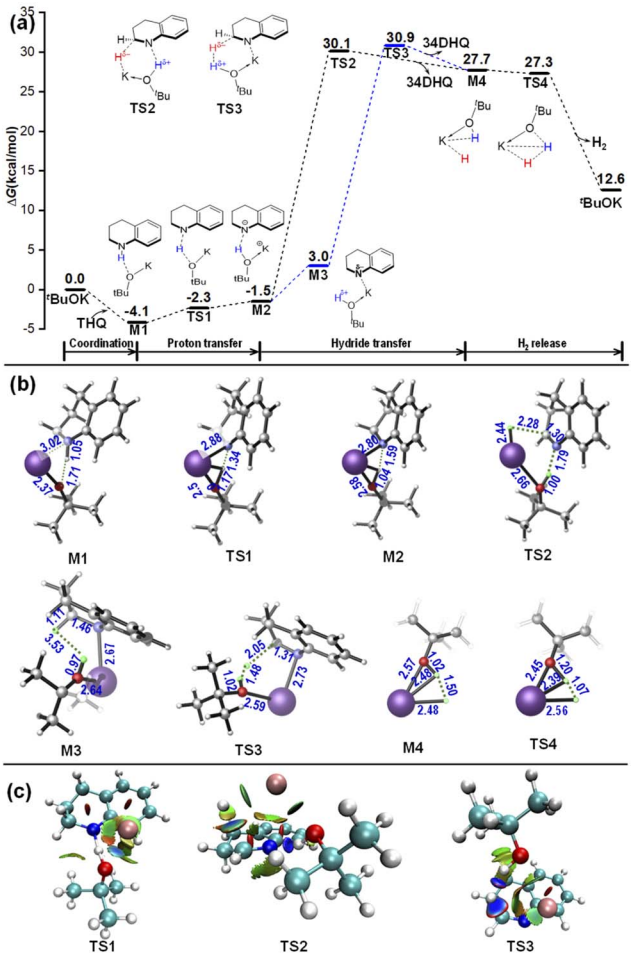

Fig. 1 (a) Relative free energy profiles for the dehydrogenation reaction of **THQ** catalyzed by ^{t}BuOK in *o*-xylene. (b) Geometrical information. (c) NCI analyses of **TS1-3**. Energies are in kcal mol^{-1}, bond distances are in angstroms.

indicating that the hydride abstraction is prone to take place from the axial C2–H2a bond.

As shown in Fig. 1c, NCI analysis shows that **TS2** is mainly stabilized by N···H–O hydrogen-bonding and C···H···K^{+} weak interactions. Taking the above proton and hydride transfer steps together, and regarding the K^{+} as a metal center and the ^{t}BuO^{-} as a ligand like in the well-established bifunctional transition metal complex catalysts, the six-membered-ring **TS2** is structurally similar with the Noyori-type metal–ligand bifunctional transition state (**TS$_{MLC}$** in Scheme 2) along an outer-sphere pathway.[23,33,34] The first dehydrogenation process through sequential **TS1** and **TS2** can be attributed to be a stepwise (proton then hydride) pathway, where a proton migrates to ^{t}BuO^{-} and a hydride transfers to K^{+}. Note that both the concerted and stepwise proton/hydride transfer pathways were taken into consideration at first. However, all attempts to locate a transition state for the concerted mechanism failed. In addition, the transition state for sequential hydride and proton transfer, *i.e.* the H2a on C2 first shifts to the ^{t}BuO^{-} before proton transfer, could also not be located. Therefore, the only feasible mechanism is the stepwise outer-sphere proton and hydride transfer pathway.

Besides the above-mentioned quasi-metal–ligand functional pathway *via* **TS2**, another competing base-catalyzed type pathway was also identified. In this case, a precursor intermediate **M3** stabilized by the N$^{\delta-}$···K$^{\delta+}$ coordination should be first formed, and is 4.5 kcal mol^{-1} higher than **M2**. Then, hydride migration can take place through **TS3**. This calculated pathway was initially inspired by the mechanism proposed by Liu *et al.*[18] However, different from the transition state **TS$_{HH}$** (*i.e.* **C** in ref. 19, see Scheme 1), there is no O···H···C hydrogen-bonding interaction found in **TS3**, but instead the N$^{\delta-}$···K$^{\delta+}$ weak interaction and the O$^{\delta-}$–H$^{\delta+}$···H$^{\delta-}$···C$^{\delta+}$ hydrogen-bonding interaction play vital roles in stabilizing the **TS3** as indicated by NCI analyses (see Fig. 1c). Interestingly, this H–H bridging transition state is structurally similar with the H–H bond cleavage transition state in based-catalyzed hydrogenation (**TS$_{BC}$** in Scheme 2) proposed by Berkessel *et al.*,[22,35] and more specifically it is analogous with the reverse pathway of the stepwise ^{t}BuOK catalyzed hydrogenation calculated by Dub *et al.*[24] In this case, the hydride is abstracted by the proton on ^{t}BuOK(H$^{\delta+}$) unit, while the K^{+} is coordinated with N atom stabilizing the **TS3** according to the NCI diagram. The corresponding energy barrier is calculated to be 0.8 kcal mol^{-1} (0.7 kcal mol^{-1} refined at B3LYP-D3/def2-QZVP level of theory) higher than that *via* **TS2**, indicating that the two Noyori- and base-catalyzed type hydride transfer pathways may coexist and the former one is slightly more superior. No matter in which case the reaction takes place, with the departure of H2a, the configuration of C2 atom changes from sp^{3} into sp^{2}, resulting in the 3,4-dihydroquinoline (**34DHQ**) and the dihydride species KO^{t}Bu(H)(H), *i.e.* the **M4** in Fig. 1, composed of a contact ion pair of KH and a *tert*-butanol. This dihydride species is also the precursor for the hydrogen release in the next step.

The H_2 elimination from O and K^{+} sites within the dihydride species occurs along a downhill pathway, regenerating the ^{t}BuOK base catalyst. The sum of free energies of the final products (**34DHQ** + ^{t}BuOK + H_2) are calculated to be endothermic by 12.6 kcal mol^{-1} relative to the separated species (**THQ** + ^{t}BuOK). Although the overall dehydrogenation reaction is thermodynamically unfavorable, it is generally entropically favored due to the H_2 liberation.

3.2. The second dehydrogenation from dihydroquinoline (DHQ) to quinoline (Q)

Once the **34DHQ** is produced, the second dehydrogenation may subsequently occur on the C3–C4 bond site. Alternatively, it may also take place on the N1 and C4 sites when **34DHQ** is converted to **14DHQ** by isomerization, or on the N1–C2 bond again if the N1=C2 double bond in **34DHQ** can be shifted to the C3–C4 position to give the **12DHQ**, the details are shown as follows.

3.2.1. Dehydrogenation from 34DHQ and 14DHQ. As illustrated in Fig. 2a, a new encounter complex **M5** may subsequently form between **34DHQ** and ^{t}BuOK stabilized by the K^{+}···π and C–H···O hydrogen bond non-covalent interactions. As a result, the C3–H3a bond is slightly activated with 0.01 Å

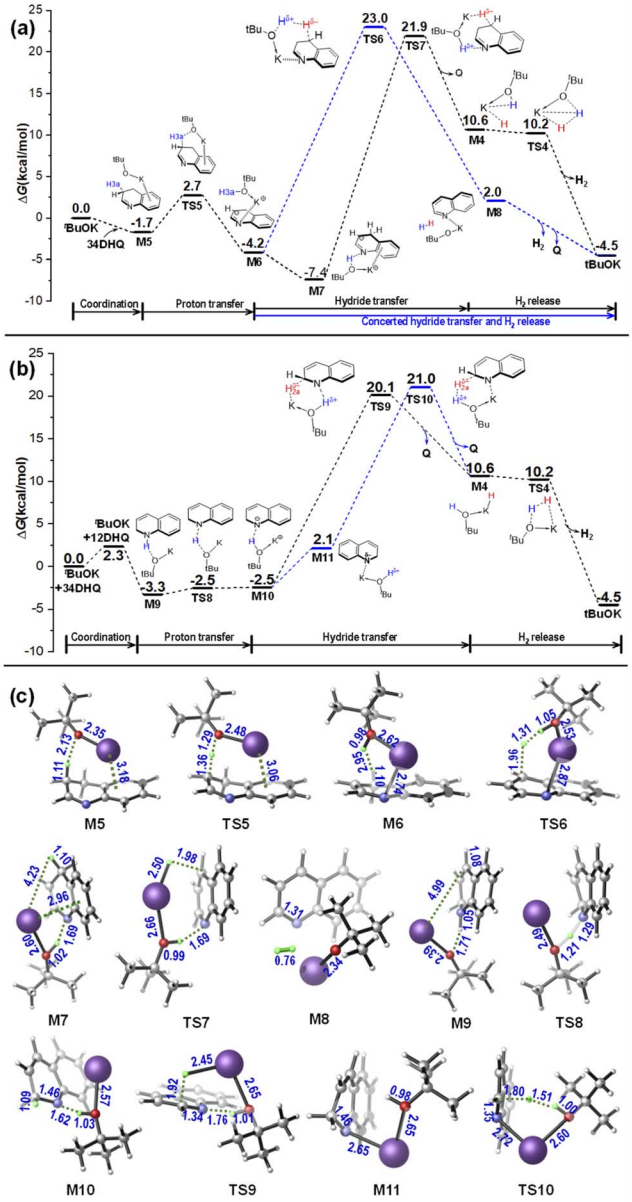

Fig. 2 Relative free energy profiles for the dehydrogenation reaction of **34DHQ** (a) and **12DHQ** (b) catalyzed by ^{t}BuOK in *o*-xylene. (c) Geometrical information. Energies are in kcal mol^{-1}, bond distances are in angstroms.

elongation. Then, the proton migrates from C3 to the O atom on ^{t}BuOK *via* **TS5** with a small energy barrier of 4.4 kcal mol^{-1}, affording the ion-pair complex **M6**. In contrast to the dehydrogenation catalyzed by transition metal complexes, in which the energy barrier for proton transfer from C3 site was calculated to be 22.8 kcal mol^{-1} mediated by a Fe-PNP catalyst,[20b] and as high as 41.2 to 47.2 kcal mol^{-1} catalyzed by a Cp*Ir complex as reported by Wang[20a] and Zhang[36] *et al.*, the corresponding process in this studied system is so facile due to the strong protophilic ability of the ^{t}BuO^{-} group.

Then starting from **M6**, hydride migrates from C4 site *via* the base-catalyzed type H–H bridging **TS6**, which is structurally similar with **TS3** in the first dehydrogenation reaction, but is evidently more stable with an energetic span of 27.2 kcal mol^{-1}. Moreover, H_2 elimination takes place synchronously with the hydride transfer, without the formation of a dihydride intermediate. Alternatively, the ion-pair complex **M6** can rearrange to be the N···H–O hydrogen bonded complex **M7** by releasing energy of 3.5 kcal mol^{-1}. The hydride transfer subsequently occurs along the quasi-metal–ligand bifunctional pathway *via* **TS7**, the energetic span of which is slightly smaller (2.1 kcal mol^{-1}) than **TS6**, indicating that the two pathways my also coexist and the Noyori-type one is slightly more facile. The quinoline (**Q**) is obtained after passing through **TS7**, delivering the dihydride intermediate **M4**. Finally, H_2 liberation and catalyst regeneration can be achieved *via* a barrierless pathway as that in the first dehydrogenation process.

The **14DHQ** can be obtained through proton transfer from ^{t}BuOH to the N1 site within the intermediate **M7**, where the ^{t}BuOH acts as a proton shuttle to facilitate the tautomerization between **34DHQ** and **14DHQ** (see Fig. S2 of ESI†). Then, to carry out the dehydrogenation from **14DHQ**, a reverse proton transfer from N1 site of **14DHQ** to ^{t}BuOK should occur to form the ion-pair complex **M7** again, and the subsequent hydride transfer is same as discussed above for **34DHQ**. In other words, an additional reversible proton transfer subprocess between **14DHQ** and **M7** is embedded in this case compared with the dehydrogenation pathway of **34DHQ**.

3.2.2. Dehydrogenation from 12DHQ. Assuming that the **12DHQ** can be formed by isomerization of **34DHQ**, the dehydrogenation process of **12DHQ** would be similar with that of **THQ**. As shown in Fig. 2b, the outer- and inner-sphere dehydrogenation pathways of **12DHQ** are determined to have energetic spans of 23.4 and 24.3 kcal mol^{-1}, respectively, which are slightly lower than that required for the dehydrogenation from **34DHQ**. However, it was suggested by Wang *et al.* that the isomerization between **34DHQ** and **12DHQ** can be achieved through by disproportionation with the assistance of proton species involving **34DHQH**$^{+}$ and **QH**$^{+}$,[20] which would be unlikely as the proton mediator is absent under alkaline conditions in the presence of ^{t}BuOK.

According to the above calculated results in Sections 3.1 and 3.2, the rate determining step of the dehydrogenation of **THQ** is the hydride transfer from C2 of **THQ** to ^{t}BuOK during the first dehydrogenation process, which may proceed along a quasi-metal–ligand bifunctional pathway *via* a six-membered-ring rate-determining **TS2**, or along a base-catalyzed pathway *via* a H–H bridging rate-determining **TS3**, which are analogous with the reverse processes of the hydrogenation mechanisms proposed by Noyori[23] and Berkessel,[22] respectively. The second dehydrogenation from **DHQ** is found to be achieved directly from **34DHQ** without the need of isomerization, and is both kinetically and thermodynamically more favourable due to the enhanced aromaticity. As a significant result, once dehydrogenation of **THQ** is triggered, only the fully dehydrogenated product **Q** will be delivered, as observed experimentally.[18]

Compared with the dehydrogenation mechanism of **THQ** mediated by transition metal catalysts such as Fe-PNP and Cp*Ir complexes as reported by Wang[20a] and

Surawatanawong[20b] *et al.*, on one hand, hydride transfer in the first dehydrogenation is the rate-determining step in all the three systems, though the hydride shift occurs before the proton transfer when using the Cp*Ir catalyst. On the other hand, proton transfer in this ^{t}BuOK catalyzed system is much more facile than the other two cases, which can be attributed to the strong protonophilic ability of ^{t}BuO^{-} group. Subsequently, as a result that for the second dehydrogenation from **DHQ**, isomerization between **34DHQ** and **12DHQ** *via* disproportionation is required to shift the double bond from N–C2 to the C3–C4, using the Cp*Ir catalyst, because proton abstraction from C3 of **34DHQ** is unlikely with high energy barrier; while it can take place directly from **34DHQ** with a proton-transfer rate-determining step, using the Fe-PNP catalyst; and in this work with a ^{t}BuOK as the catalyst, we found it can occur also directly from **34DHQ**, but hydride migration is the rate-determining step.

3.3. Effect of nitrogen substituent for THQ dehydrogenation

To explore the regulation effect of the nitrogen substituent, similar process of 1,2,3,4-tetrahydronaphthalene (**THNap**) catalyzed by ^{t}BuOK was also investigated, as shown in Fig. 3. Different from the case for **THQ**, the first dehydrogenation of **THNap** is so slow that an energetic span as high as 43.1 to 43.6 kcal mol^{-1} along the two type pathways should be overcome. On one side, a moderate energy barrier of 15.1 kcal mol^{-1} was determined for the proton transfer from C1 on **THNap** to oxygen atom on ^{t}BuOK, which becomes more difficult compared to that for **THQ** due to the N–H bond in **THQ** is weaker than the C–H bond in **THNap**.[2c] On the other hand, the hydride transfer from C2 of **THNap** becomes more thermodynamically unfavorable than that for **THQ**, because the C2–H bond adjacent to the N1 site in **THQ** also gets weaker. In short, the incorporation of N-heteroatom can facilitate both the proton transfer and especially the hydride transfer processes. In addition, compared with the dehydrogenation of **THNap** catalyzed by the Fe(II) complex in which the proton transfer step was reported to be the rate-determining step with an energy barrier of 42.2 kcal mol^{-1},[20b] the rate-determining step in this case is the hydride transfer step whereas the proton transfer is relatively feasible. The total results show that the nitrogen substituent is also necessary for dehydrogenation reaction promoted by the ^{t}BuOK base catalyst.

3.4. Dehydrogenation of THQ catalyzed by ^{t}BuO^{-} and ^{t}BuOLi

To further explore the effect of alkali ion, the reaction pathways catalyzed an isolated ^{t}BuO^{-} anion (see Fig. S3†) and by a ^{t}BuOLi base were also calculated (see Fig. 4). Given that the first dehydrogenation of **THQ** is rate-determining, only the pathways of first dehydrogenation from **THQ** in these cases were studied.

The relative free energy profiles for the dehydrogantion of **THQ** catalyzed by an isolated ^{t}BuO^{-} is plotted in Fig. S3.† Note that without the involvement of any alkali ion, only the base-catalyzed mechanism was considered in this case. The

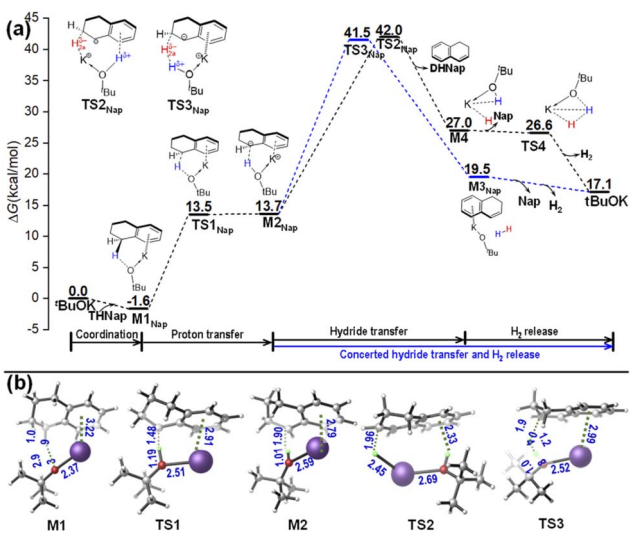

Fig. 3 (a) Relative free energy profiles for the dehydrogenation reaction of 1,2,3,4-tetrahydronaphthalene (THNap) catalyzed by ^{t}BuOK in *o*-xylene. (b) Geometrical information. Energies are in kcal mol^{-1}, bond distances are in angstroms.

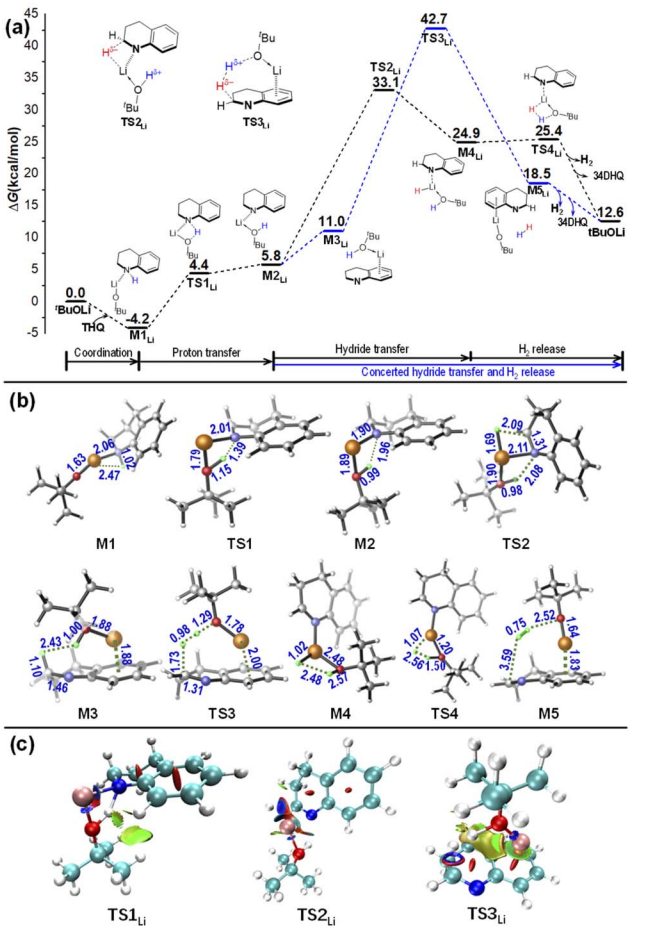

Fig. 4 (a) Relative free energy profiles for the dehydrogenation reaction of **THQ** catalyzed by ^{t}BuOLi in *o*-xylene. (b) Geometrical information. (c) NCI analyses of **TS1-3**. Energies are in kcal mol^{-1}, bond distances are in angstroms.

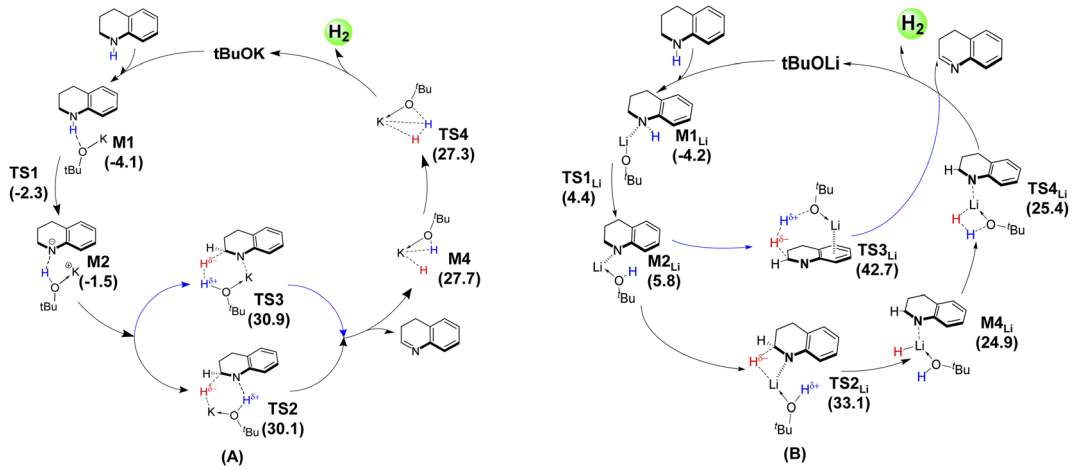

Scheme 3 Summary of catalytic cycles for the dehydrogenation from THQ mediated by the ^{t}BuOK (A) and ^{t}BuOLi (B) base catalysts.

calculated energetic span is as high as 40 kcal mol^{-1} *via* **TS2$_t$**, suggesting that the K$^+$ ion plays vital role in stabling the transition state and facilitating the dehydrogenation reaction.

As shown in Fig. 4, in the case of using ^{t}BuOLi as the catalyst, the associated complexes **M1$_{Li}$** is stabled by Li$^+$⋯N covalent interaction, and no presence of N–H⋯O hydrogen bond like the cases of using ^{t}BuOK as the catalyst. As a result, the barrier for proton transfer becomes obviously higher. In addition, different from the six-membered-ring quasi-Noyori-type **TS2** along the metal–ligand bifunctional pathway mediated by ^{t}BuOK, the **TS2$_{Li}$** exhibits a four-membered-ring interaction according to the structural information and NCI analyses in Fig. 4 *versus* that in Fig. 2. Further bonding analyses were also done using the ETS-NOCV method. The NOCV analyses illustrated in Fig. S5† reveal that there is evident binding interaction between N atom and Li$^+$ (in **M2$_{Li}$** and **TS2$_{Li}$**) but not with the case of ^{t}BuOK$^+$, indicating that the small size as well as strong Lewis acidity of Li$^+$ allows for effective binding to N atom and prevention of non-covalent interaction for hydride transfer.[37] Correspondingly, the energy barrier for hydride transfer *via* the four-membered **TS2$_{Li}$** is determined to be 37.3–38.8 kcal mol^{-1} (obtained by using B3LYP-D3 functional with def2-TZVP and def2-QZVP basis sets), and is 3.1–4.3 kcal mol^{-1} higher than that *via* the six-membered **TS2** catalyzed by ^{t}BuOK.

Another possible process along the base-catalyzed-type pathway was also examined. The results show that a high energy barrier of 46.9–48.9 kcal mol^{-1} (obtained by using B3LYP-D3 functional with def2-TZVP and def2-QZVP basis sets) is required by using a ^{t}BuOLi catalyst. Structurally different from the **TS3(K)**, the Li$^+$ binds to phenyl ring of **THQ** *via* cation⋯π interaction with **TS3$_{Li}$** (see Fig. 3). In addition, it takes places along a concerted hydride transfer and H_2 release channel *via* the H–H bridging transition state **TS3$_{Li}$**, and C–H and O–H bonds are simultaneously broken, leading to a remarkably high energy barrier. Interestingly, it was reported by Dub *et al.* that in the ketone hydrogenation reaction promoted by ^{t}BuOK, the H–H bond cleavage and the hydride transfer show a concert behaviour in gas phase, while it is stepwise with a lower energy barrier in solution phase.[24a] This work also suggests that the stepwise behaviour in the presence of ^{t}BuOK can facilitate the reaction in the framework of the base-catalyzed type mechanism.

Based on the above data and discussions, a mechanism diagram can be drawn for comparison of the dehydrogenation of **THQ** catalyzed by ^{t}BuOK *vs.* ^{t}BuOLi, as shown in Scheme 3. It is clearly seen that both the quasi-metal–ligand pathway and the base-catalyzed type channel catalyzed by ^{t}BuOLi are energetically higher than that mediated by ^{t}BuOK. In particular, the base-catalyzed type one *via* **TS3$_{Li}$** is infeasible with a remarkably large energetic span. These calculated results provide a clearly physical picture to explain why the experimentally observed yield was sharply dropped when using ^{t}BuOLi (19%) instead of ^{t}BuOK (99%) as the catalyst.[18]

4. Conclusions

This DFT computational study provides mainly the following insights into the ADH of **THQ** catalyzed by an alkali catalyst of ^{t}BuOK *versus* ^{t}BuOLi as a case study:

(1) This work reveals that the dehydrogenation mediated by ^{t}BuOK can proceed efficiently along a quasi-metal–ligand bifunctional catalytic channel or a base-catalyzed pathway with close energy barriers.

(2) No matter which pathway the reaction follows, the hydride transfer in the first dehydrogenation process is the rate determining step. The second dehydrogenation is found to be achieved directly from **34DHQ** regulated by a ^{t}BuOK catalyst, without the need of further isomerisation.

(3) In contrast, for the case in presence of the ^{t}BuOLi catalyst, the concerted hydride transfer and H_2 elimination along a base-catalyzed pathway is infeasible with a significantly high energy barrier. Thus, the dehydrogenation can only proceed along the quasi-metal–ligand bifunctional pathway with a relatively higher barrier, due to binding of N atom weakens the affinity of Li$^+$ for hydride abstraction. This is consistent with the experimental observation that ^{t}BuOLi is inferior to ^{t}BuOK as a dehydrogenation catalyst.

In short, this work contributes to a comprehensive understanding of the ADH catalyzed by a simple base catalyst, which may provide help in the rational design of new catalysts for the ADH reactions as well as the LOHC systems.

Conflicts of interest

The authors declare no competing financial interest.

Acknowledgements

We are grateful to the supports from the National Natural Science Foundation of China (NSFC22003076, NSFC21576291), the Natural Science Foundation of Shandong Province (ZR2020MB023), the Fundamental Research Funds for the Central Universities (22CX06012A, 20CX06031A) and the Qingdao Postdoctoral Applied Research Project (QDYY20190035).

References

1 (*a*) M. Niermann, S. Timmerberg, S. Drünert and M. Kaltschmitt, *Renewable Sustainable Energy Rev.*, 2021, **135**, 110171; (*b*) P. Preuster, C. Papp and P. Wasserscheid, *Acc. Chem. Res.*, 2017, **50**, 74–85; (*c*) Z. X. Giustra, J. S. A. Ishibashi and S.-Y. Liu, *Coord. Chem. Rev.*, 2016, **314**, 134–181; (*d*) M. Niermann, A. Beckendorff, M. Kaltschmitt and K. Bonhoff, *Int. J. Hydrogen Energy*, 2019, **44**, 6631–6654.

2 (*a*) E. Clot, O. Eisenstein and R. H. Crabtree, *Chem. Commun.*, 2007, 2231–2233; (*b*) A. Moores, M. Poyatos, Y. Luo and R. H. Crabtree, *New J. Chem.*, 2006, **30**, 1675–1678; (*c*) R. H. Crabtree, *Energy Environ. Sci.*, 2008, **1**, 134–138; (*d*) R. H. Crabtree, *ACS Sustainable Chem. Eng.*, 2017, **5**, 4491–4498.

3 (*a*) Y. Zhang, J. Wang, F. Zhou and J. Liu, *Catal. Sci. Technol.*, 2021, **11**, 3990–4007; (*b*) K. C. Tan, T. He, Y. S. Chua and P. Chen, *J. Phys. Chem. C*, 2021, **125**, 18553–18566.

4 C. Gunanathan and D. Milstein, *Science*, 2013, **341**, 1229712.

5 T. Shimbayashi and K.-I. Fujita, *Tetrahedron*, 2020, **76**, 130946.

6 (*a*) R. Yamaguchi, C. Ikeda, Y. Takahashi and K. Fujita, *J. Am. Chem. Soc.*, 2009, **131**, 8410–8412; (*b*) K. Fujita, Y. Tanaka, M. Kobayashi and R. Yamaguchi, *J. Am. Chem. Soc.*, 2014, **136**, 4829–4832; (*c*) K. Fujita, T. Wada and T. Shiraishi, *Angew. Chem., Int. Ed.*, 2017, **56**, 10886–10889.

7 (*a*) D. Talwar, A. Gonzalez-de-Castro, H. Y. Li and J. Xiao, *Angew. Chem., Int. Ed.*, 2015, **54**, 5223–5227; (*b*) J. Wu, D. Talwar, S. Johnston, M. Yan and J. Xiao, *Angew. Chem., Int. Ed.*, 2013, **52**, 6983–6987; (*c*) B. Maji, A. Bhandari, D. Bhattacharya and J. Choudhury, *Organometallics*, 2022, **41**(13), 1609–1620.

8 (*a*) R. Xu, S. Chakraborty, H. Yuan and W. D. Jones, *ACS Catal.*, 2015, **5**, 6350–6354; (*b*) S. Chakraborty, W. W. Brennessel and W. D. Jones, *J. Am. Chem. Soc.*, 2014, **136**, 8564–8567.

9 O. R. Luca, D. L. Huang, M. K. Takase and R. H. Crabtree, *New J. Chem.*, 2013, **37**, 3402.

10 Q. F. Wang, H. N. Chai and Z. K. Yu, *Organometallics*, 2018, **37**, 584–591.

11 P. Sánchez, M. Hernández-Juárez, N. Rendón, J. López-Serrano, L. L. Santos, E. Álvarez, M. Paneque and A. Suárez, *Dalton Trans.*, 2020, **49**, 9583–9587.

12 (*a*) M. A. Esteruelas, V. Lezáun, A. Martínez, M. Oliván and E. Oñate, *Organometallics*, 2017, **36**, 2996–3004; (*b*) M. L. Buil, M. A. Esteruelas, M. P. Gay, M. Gómez-Gallego, A. I. Nicasio, E. Oñate, A. Santiago and M. A. Sierra, *Organometallics*, 2018, **37**, 603–617.

13 G. Jaiswal, V. G. Landge, D. Jagadeesan and E. Balaraman, *Nat. Commun.*, 2017, **8**, 1–13.

14 (*a*) Y. Han, Z. Wang, R. Xu, W. Zhang, W. Chen, L. Zheng, J. Zhang, J. Luo, K. Wu, Y. Zhu, C. Chen, Q. Peng, Q. Liu, P. Hu, D. Wang and Y. Li, *Angew. Chem., Int. Ed.*, 2018, **57**, 11262–11266; (*b*) G. Jaiswal, M. Subaramanian, M. K. Sahoo and E. Balaraman, *ChemCatChem*, 2019, **11**, 2449–2457.

15 Z. Zhang, W. Liu, Y. Zhang, J. Bai and J. Liu, *ACS Catal.*, 2021, **11**, 313–322.

16 (*a*) H. T. Hu, Y. Q. Nie, Y. W. Tao, W. Y. Huang, L. Qi and R. F. Nie, *Sci. Adv.*, 2022, **8**, 9478; (*b*) A. Mollar-Cuni, D. Ventura-Espinosa, S. Martín, H. García and J. A. Mata, *ACS Catal.*, 2021, **11**, 14688–14693.

17 (*a*) M. Kojima and M. Kanai, *Angew. Chem., Int. Ed.*, 2016, **128**, 12412–12415; (*b*) S. Tamke, Z.-W. Qu, N. A. Sitte, U. Flörke, S. Grimme and J. Paradies, *Angew. Chem., Int. Ed.*, 2016, **55**, 12219–12223.

18 T. Liu, K. Wu, L. Wang and Z. Yu, *Adv. Synth. Catal.*, 2019, **361**, 3958–3964.

19 H. Li and Z. Wang, *Sci. China: Chem.*, 2012, **55**, 1991–2008.

20 (*a*) H. Li, J. Jiang, G. Lu, F. Huang and Z.-X. Wang, *Organometallics*, 2011, **30**, 3131–3141; (*b*) B. Sawatlona and P. Surawatanawong, *Dalton Trans.*, 2016, **45**, 14965; (*c*) S. M. Bellows, S. Chakraborty, J. B. Gary, W. D. Jones and T. R. Cundari, *Inorg. Chem.*, 2017, **56**, 5519–5524.

21 A. Bera, S. Bera and D. Banerjee, *Chem. Commun.*, 2021, **57**, 13042–13058.

22 A. Berkessel, T. J. S. Schubert and T. N. Muller, *J. Am. Chem. Soc.*, 2002, **124**, 8693–8698.

23 (*a*) M. Yamakawa, H. Ito and R. Noyori, *J. Am. Chem. Soc.*, 2000, **122**, 1466–1478; (*b*) R. Noyori, *Adv. Synth. Catal.*, 2003, **345**, 15–32.

24 (*a*) P. A. Dub and N. V. Tkachenko, *J. Phys. Chem. A*, 2021, **125**, 5726–5737; (*b*) P. A. Dub, *Eur. J. Inorg. Chem.*, 2021, **47**, 4884–4889.

25 (*a*) C. Lee, W. Yang and R. G. Parr, *Phys. Rev. B: Condens. Matter Mater. Phys.*, 1988, **37**, 785–789; (*b*) A. D. Becke, *J. Chem. Phys.*, 1993, **98**, 1372–1377.

26 S. Grimme, J. Antony, S. Ehrlich and H. Krieg, *J. Chem. Phys.*, 2010, **132**, 154104.

27 (*a*) A. Schäfer, C. Huber and R. Ahlrichs, *J. Chem. Phys.*, 1994, **100**, 5829–5835; (*b*) K. Eichkorn, F. Weigend, O. Treutler and R. Ahlrichs, *Theor. Chem. Acc.*, 1997, **97**, 119–124.

28 M. J. Frisch, G. W. Trucks, H. B. Schlegel, G. E. Scuseria, M. A. Robb, J. R. Cheeseman, G. Scalmani, V. Barone, B. Mennucci, G. A. Petersson, H. Nakatsuji, M. Caricato,

X. Li, H. P. Hratchian, A. F. Izmaylov, J. Bloino, G. Zheng, J. L. Sonnenberg, M. Hada, M. Ehara, K. Toyota, R. Fukuda, J. Hasegawa, M. Ishida, T. Nakajima, Y. Honda, O. Kitao, H. Nakai, T. Vreven, J. A. Montgomery Jr, J. E. Peralta, F. Ogliaro, M. Bearpark, J. J. Heyd, E. Brothers, K. N. Kudin, V. N. Staroverov, R. Kobayashi, J. Normand, K. Raghavachari, A. Rendell, J. C. Burant, S. S. Iyengar, J. Tomasi, M. Cossi, N. Rega, J. M. Millam, M. Klene, J. E. Knox, J. B. Cross, V. Bakken, C. Adamo, J. Jaramillo, R. Gomperts, R. E. Stratmann, O. Yazyev, A. J. Austin, R. Cammi, C. Pomelli, J. W. Ochterski, R. L. Martin, K. Morokuma, V. G. Zakrzewski, G. A. Voth, P. Salvador, J. J. Dannenberg, S. Dapprich, A. D. Daniels, Ö. Farkas, J. B. Foresman, J. V. Ortiz, J. Cioslowski and D. J. Fox, *Gaussian 09, revision D.01*, Gaussian Inc., Wallingford, CT, 2013.

29 T. Lu and F. Chen, *J. Comput. Chem.*, 2012, **33**, 580–592.

30 (*a*) I. D. Jenkins and E. H. Krenske, *ACS Omega*, 2020, **5**, 7053–7058; (*b*) M. G. Stanton, C. B. Allen, R. M. Kissling, A. L. Lincoln and M. R. Gagné, *J. Am. Chem. Soc.*, 1998, **120**, 5981–5989; (*c*) P. Hima, M. Vageesh, M. Tomasini, A. Poater and R. Dey, *Mol. Catal.*, 2023, **542**, 113110.

31 (*a*) L. Zhang, H. Yang and L. Jiao, *J. Am. Chem. Soc.*, 2016, **138**, 7151–7160; (*b*) G. Nocera, A. Young, F. Palumbo, K. J. Emery, G. Coulthard, T. McGuire, T. Tuttle and J. A. Murphy, *J. Am. Chem. Soc.*, 2018, **140**, 9751–9757.

32 S. Kozuch and S. Shaik, *Acc. Chem. Res.*, 2010, **44**, 101–110.

33 (*a*) C. Hou, Z. Zhang, C. Zhao and Z. Ke, *Inorg. Chem.*, 2016, **55**, 6539–6551; (*b*) K. T. Tseng, J. W. Kampf and N. K. Szymczak, *ACS Catal.*, 2015, **5**, 5468–5485; (*c*) G. Zeng, S. Sakaki, K. Fujita, H. Sano and R. Yamaguchi, *ACS Catal.*, 2014, **4**, 1010–1020.

34 P. A. Dub and J. C. Gordon, *Nat. Chem. Rev.*, 2018, **2**, 396–408.

35 B. Chan and L. Radom, *J. Am. Chem. Soc.*, 2005, **127**, 2443–2454.

36 X.-B. Zhang and X. Zhao, *Phys. Chem. Chem. Phys.*, 2011, **13**, 3997–4004.

37 Y.-W. Zhao, H.-R. Zhu, S.-Y. Sung, D. J. Wink, J. M. Zadrozny and T. G. Driver, *Angew. Chem., Int. Ed.*, 2021, **60**, 19207–19213.